2014 IEEE International Conference on Robotics & Automation (ICRA)
Hong Kong Convention and Exhibition Center
May 31 - June 7, 2014. Hong Kong, China

Expanding Workspace of Underactuated Flexible Manipulators by Actively Deploying Constraints

Zheng Li *Member IEEE, ASME* and Ruxu Du *Fellow ASME, SME, HKIE*

***Abstract* — This paper presents the idea of employing constraints to expand the workspace of Underactuated Flexible Manipulators (UFM). The constraints are divided into two types: bilateral constraint (BC) and unilateral constraint (UC). Under the constraints the UFM is segmented into two sections: the anterior constrained section and the distal free section; moreover, the motion of the UFM is altered, i.e., the end effector of the UFM can get access to positions where unreachable previously, or, the workspace is expanded. In the paper, constrained kinematics model is developed at first. The workspace is derived thereafter. To validate the idea, an underactuated wire-driven serpentine manipulator is built. In the experiments, the two types of constraints are applied. Experiment results agree well with the simulation results.**

I. INTRODUCTION

ROBOT arm is widely used. From the structure point of view, it could be divided into three categories, i.e. discrete robotic arm, serpentine robotic arm and continuum robotic arm [1]. A discrete robotic arm has a few rigid links, such as SCARA and PUMA robot. This type of manipulator has limited Degree of Freedoms (DOFs) and is usually operated in open space. A serpentine robotic arm has a series of chained links [2-4]. The DOF number is increased a lot. A continuum robotic arm has several compliant segments with a few joints [5] or no joint at all [6]. Theoretically, the DOF number is infinite. Serpentine robotic arms and continuum robotic arms are both flexible and are categorized as flexible manipulator.

To fully control the flexible manipulator, a large number of actuators are needed. This makes the manipulator structure as well as the control very complicated. Underactuation [7, 8] could simplify the robot system a lot. In the underactuated system, the actuator number is less than the number of DOFs. As a consequence, workspace of the manipulator is reduced. Typical underactuated flexible manipulators (UFM) are Wire/Tendon/Cable driven serpentine robotic arms and continuum robotic arms [2, 5, 9]. End effector of the UFM is positioned and orientated by bending the backbone actively. During the bending, the joints rotations are related.

Due to the flexibility, UFMs are well suited in confined space. Typical applications are Minimally Invasive Surgery (MIS), engineering non-destructive inspection, disaster relief etc.[10]. The "Snake Arm" of OC Robotics [11], is a typical UFM used for engineering inspection. During the inspection, the flexible manipulator is inserted into the target area, such as the engine cavity. The position and orientation of the end effector is controlled by tendons. Images inside the engine are transmitted to the monitor. However, not every region inside the cavity can be viewed due to the limited workspace. Conventionally, obstacles are avoided in the operation. This would further reduce the workspace of the robot. To avoid the obstacles and plan the robot motion in confined space, researchers have already worked out a lot of approaches. Such as in [3] and [12] motion planning methods are proposed for flexible manipulators.

Indeed, obstacles hinder the robot movement. Though, we can also take advantage of them. In nature, there are a lot of underactuated flexible examples, such as snake, octopus arm, human fingers, and etc. How do they employ the obstacles? Take the human index finger as an example. Similar to UFMs, the motion of the finger is flexing. Without external forces, the index finger cannot flex the distal inter-phalangeal joint only, at least for the author. This shows the index finger can employ the external constraint bending to different shapes. For a UFM, new shapes mean additional end effector position and orientation. In the inspection, it is always beneficial that the instrument can reach more positions or reach the same position with more orientation options. In this paper, the novel idea of employing obstacles to expand UFM workspace is presented. Examples are given by the underactuated wire-driven serpentine robotic arm with one bending DOF.

The rest of the paper is organized as follows: in section 2 the design as well as the kinematics model of UFMs are reviewed; in section 3 constrained kinematics model for UFMs is derived; in section 4 the workspace of UFMs with two types of constraints are developed; in section 5 the wire-driven robotic arm as well as experiment results are presented; finally, conclusions are given in section 6.

II. UNDERACTUATED FLEXIBLE MANIPULATOR

There are two types of UFMs. One is the underactuated continuum manipulator (UCM), such as the "Elephant Trunk Robot" [13]. The other is the underactuated serpentine manipulator (USM), such as the "Snake Arm"[11]. The actuation of UFM can be various, such as Pneumatic Artificial Muscle (PAM) [13], Shape Memory Alloy (SMA) [14], Electro Active Polymer (EAP) [15], wire / tendon / cable [9, 16], etc. Figure 1 shows the backbone deformation of the two types of UFMs.

Zheng Li and Ruxu Du are with the Institute of Precision Engineering and the Dept. of Mechanical and Automation Engineering, the Chinese University of Hong Kong, Hong Kong SAR (phone: 852-31634237; email: zli@mae.cuhk.edu.hk, rdu@mae.cuhk.edu.hk).

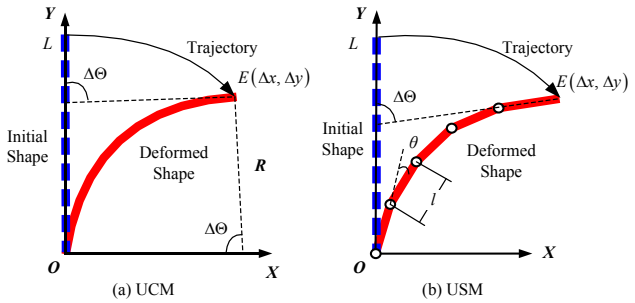

Fig.1 Two types of UFMs

For UFMs, to reach a target position their backbones are deformed to a specific configuration by the actuators. The kinematics can be divided into two parts: from the actuation space to the configuration space and from the configuration space to the task space [1]. In the first part, the kinematics model varies with actuation methods. The second part is purely geometry problem.

In this section, the kinematics model of the second part is reviewed for single segment planar UCM and USM. It is simple but fundamental. As the backbone of UFMs is usually bend to a circular arc, in the analysis, the piecewise constant curvature assumption is used. Figure 1(a) shows the UCM motion. In the figure, the blue dashed line represents the manipulator at resting position. The red curve is the deformed backbone. From the constant curvature assumption, the position of the end effector is as Equation (1). Here L is the length of the flexible backbone, $\Delta\Theta$ is the backbone bending angle, and $R=L/\Delta\Theta$ is the curve radius.

$$\begin{bmatrix}\Delta x\\ \Delta y\end{bmatrix}=\begin{bmatrix}R(1-\cos(\Delta\Theta))\\ R\sin(\Delta\Theta)\end{bmatrix} \tag{1}$$

Figure 1(b) shows the USM motion. The blue dashed line is the USM at resting position. The red polyline is the deformed USM. It is assumed that there are N links, and the length of each link is l. When the end effector orientation is controlled as $\Delta\Theta$, the end effector position is as per Equation (2).

$$\begin{bmatrix}\Delta x\\ \Delta y\end{bmatrix}=\begin{bmatrix}l\cdot\sum_{i=1}^{N}\sin(i\cdot\theta)\\ l\cdot\sum_{i=1}^{N}\cos(i\cdot\theta)\end{bmatrix} \tag{2}$$

In the equation θ is the joint rotation. Similarly, from the constant curvature assumption, the rotation of each joint is identical, i.e. $\Delta\Theta=N\cdot\theta$.

UCM could be viewed as a special case of USM when N goes to infinity. The end effector position with respect to bending angle is as shown in Equation (3). From Equation (3), the end effector rotation can be solved as per Equation (4). Equation (3) and Equation (4) are the generalized forward kinematics model and inverse kinematics model for single segment planar UFM. When the UFM structure parameters, i.e. L, N, are known, the UFM end effector position could be determined from the orientation, and vice versa.

$$\begin{bmatrix}\Delta x\\ \Delta y\end{bmatrix}=\begin{bmatrix}\frac{L}{N}\cdot\frac{\sin(\Delta\Theta/2)\cdot\sin(\Delta\Theta(N+1)/2N)}{\sin(\Delta\Theta/2N)}\\ \frac{L}{N}\cdot\frac{\sin(\Delta\Theta/2)\cdot\cos(\Delta\Theta(N+1)/2N)}{\sin(\Delta\Theta/2N)}\end{bmatrix} \tag{3}$$

$$\Delta\Theta=\frac{2N}{N+1}\arctan\left(\frac{\Delta x}{\Delta y}\right) \tag{4}$$

Workspace is the set of all reachable positions. For single segment UFMs, the workspace is the trajectory of the end effector. It is obtained from the forward kinematics model. From Equation (3), the workspace could be represented as:

$$\Delta x^2+\Delta y^2=\left(\frac{L\cdot\sin(\Delta\Theta/2)}{N\cdot\sin(\Delta\Theta/2N)}\right)^2 \tag{5}$$

where $\Theta_{\min}\le\Delta\Theta\le\Theta_{\max}$. The two limits $\Theta_{\min}$ and $\Theta_{\max}$ are determined by the UFM structure. From Equation (5), it is seen that the trajectory of a single segment UFM is quadratic.

III. Kinematics Under Constraint

In the confined space, there are two types of obstacles. One is the bilateral constraint (BC), and the other is the unilateral constraint (UC). Figure 2 shows the UFM bending motion in three cases: i) free bending; ii) bend under BC; iii) bend under UC. When the UFM is constrained, it is segmented into the anterior constrained section and the distal free section. The BC confines the free section two-sided, while the UC confines the free section one-sided.

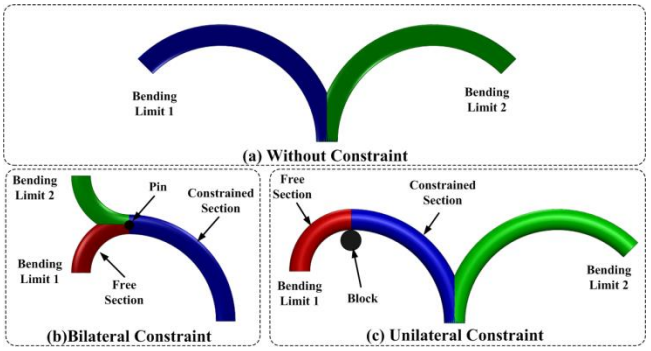

Fig. 2 Three Types of UFM Motion

In practice, there are several ways to find the constraint position, such as stereo vision [17], magnetic sensor [18], etc. Bajo and Simman also proposed a method to locate the contact for continuum robots [19]. Therefore, we assume that the constraint position (x_c, y_c) in the robot base coordinate frame is known. The kinematics under constraint can be obtained by three steps: first, find the constrained joint position and the constrained link orientation; second, perform unconstrained kinematics for the free section w.r.t. the constrained joint; third, obtain the end effector position and orientation by integrating the first two parts.

A. Constraint Forward Kinematics

Figure 3 shows the UFM under constraint. In the figure, B is the UFM base, C is the constraint. Assume there are N'

joints in the constrained section; the joint rotation is θ'; the length is $L'=N'\cdot l$; the bending angle is $\Delta\Theta_{N'}$; and the location of the constraint on link $P_{N'-1}P_{N'}$ is l'. In the free section, there are N'' joints; the joint rotation is θ''; the length is $L''=L-L'$. The overall bending angle of the UFM is $\Delta\Theta$.

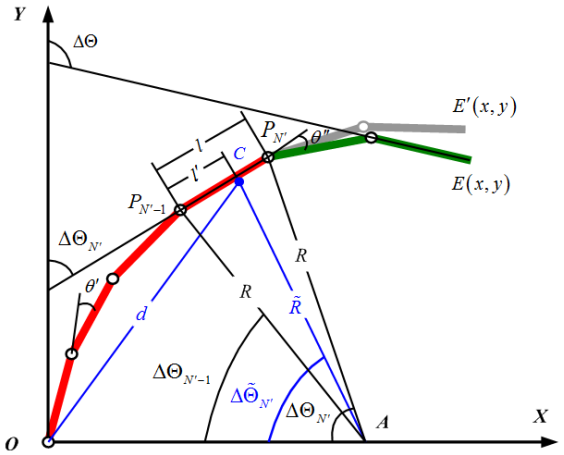

Fig. 3 Analysis of UFM Motion with Constraint

In the first step, assume the constraint position is $(x_c,\ y_c)$, and the robot base is at $(x_b,\ y_b)$. Then, the distance between the constraint and the robot base is:

$$d=\sqrt{(x_c-x_b)^2+(y_c-y_b)^2} \tag{6}$$

From Figure 3, $\Delta\tilde{\Theta}_{N'}$ is as per Equation (7), and it is obvious that $\Delta\Theta_{N'-1}\le\Delta\tilde{\Theta}_{N'}\le\Delta\Theta_{N'}$. The length of constrained section L' is initially approximated as per Equation (8).

$$\Delta\tilde{\Theta}_{N'}=\pi-2\arctan\left(\frac{y_c-y_b}{x_c-x_b}\right) \tag{7}$$

$$\tilde{L}'=\frac{d}{2\cdot\sin\left(\Delta\tilde{\Theta}_{N'}/2\right)}\Delta\tilde{\Theta}_{N'} \tag{8}$$

It can be shown that $L'\le\tilde{L}'\le L'+l$. As a result, the fixed joint number is the quotient of $\tilde{L}'$ and l. When the constrained joint number is known, the joint rotation angle could be solved from Equation (9).

$$\frac{l\cdot\sin(N'\beta)\sin[(N'-1)\beta]}{x_c\cos(2N'\beta)-y_c\sin(2N'\beta)}=\sin(\beta) \tag{9}$$

where, $\beta=\theta'/2$. The rotation of the constrained joint is $\Delta\Theta_{N'}=2N'\beta$. The constrained joint position is:

$$y_{N'}=l\cdot\frac{\sin(N'\beta)}{\sin(\beta)}\cos[(N'+1)\beta] \tag{10}$$

$$x_{N'}=l\cdot\frac{\sin(N'\beta)}{\sin(\beta)}\sin[(N'+1)\beta] \tag{11}$$

The constrained joint $P_{N'}$ is now the base of the distal free section. The free section is viewed as a new manipulator. The kinematics model is the same as the previous unconstrained kinematics, with the backbone length $L''=L-L'$ and joint number $N''=N-N'$.

B. Constraint Inverse Kinematics

The inverse kinematics is to answer the question how to reach a position with given orientation. In the constraint inverse kinematics, the problem becomes how to deploy constraints/obstacles to enable the UFM reaching the position with given orientation.

Assume the targeted end effector position is (x, y), and the desired rotation is $\Delta\Theta$. From Figure 3, it is seen that as long as the constraint lies along link $P_{N'-1}P_{N'}$, the position of $P_{N'}$ is the same. As a result, in practice, we can apply the constraint on the joint, i.e. C is coincident with $P_{N'}$. From Figure 3, the following formulas are established:

$$\begin{cases} N=N'+N'' \\ \Delta\Theta=2(N'\theta'+N''\theta'') \\ X=\dfrac{L\sin(N'\theta')}{N\sin(\theta')}\sin[(N'+1)\theta']+\dfrac{L\sin(N''\theta'')}{N\sin(\theta'')}\sin[2N'\theta'+(N''+1)\theta''] \\ Y=\dfrac{L\sin(N'\theta')}{N\sin(\theta')}\cos[(N'+1)\theta']+\dfrac{L\sin(N''\theta'')}{N\sin(\theta'')}\cos[2N'\theta'+(N''+1)\theta''] \end{cases} \tag{12}$$

In Equation (12), there are four unknowns $(N',N'',\theta',\theta'')$ and four independent equations. Mathematically, solutions exist. However, due to the UFM structure constraint, the joint rotation is bounded. As a result, only the solution that has valid joint rotation is admissible. To find the admissible solution, we can let N' varying from 1 to $N-1$ and find all the orientations. On the contrary, when orientation is of more importance, we can also find the $N-1$ possible end effector positions. It is not for sure that we can meet the position and orientation requirements simultaneously. As a compromise, we can meet one first and make the other as close as possible. Figure 4 gives an example. In this example, N=10, l=15 and Θ_{max}=142.5°. In the figures, the red dashed curve is the end effector trajectory without constraint. The left and right green poly lines are the manipulator at two bending limits. The circles denote the joints and the solid square is the constrained joint. Yellow represents effective solution, and cyan means in the solution the joint rotation violates the limit. The desired position is X=66.1mm, Y=120.7mm and the orientation is Θ=1.32rad. In Figure 4 (a), bilateral constraint is deployed at joint 1 to joint 9 successively. In all the cases, the end effector gets to the desired position. The enlarged view shows the end effector orientation. In this example, admissible solution exists when the sixth joint is constrained as shown by the red line. For the fixed joints, the rotation is 0.03 rad; the rotations of other joints are 0.12 rad. Together with the admissible solution, there are 6 orientations for the end effector to reach the target position. The cases in cyan denote the solution violates the joint limit. Figure 4 (b) shows the solutions with desired end effector orientation and X position. From the simulation results, there are totally five configurations to meet the requirement. Figure 4 (c) shows the solutions with

exact orientation and *Y* position. From the simulation results, besides the admissible solution, there are three configurations to meet the requirement. It should be noted that, admissible solution does not always exist. With increased number of links, it is more likely to have admissible solution. When *N* is infinity (i.e. UCM), admissible solution always exists.

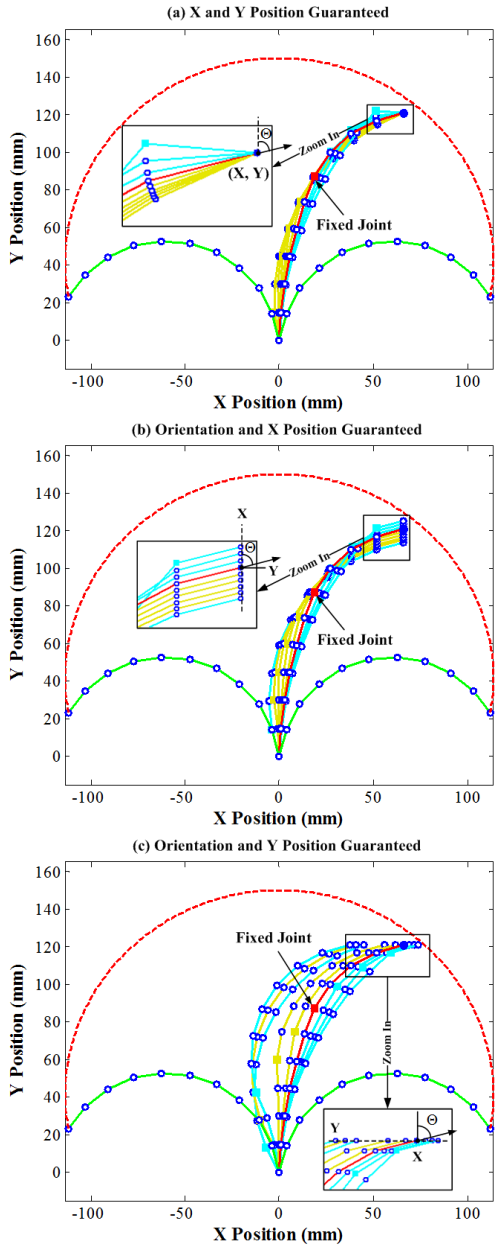

Fig.4 Constraint Deployment in three cases

IV. Workspace Under Constraint

Workspace of the UFM is obtained from the forward kinematics. It is the collection of all possible positions which the end effector can reach. The BC and UC limit the joint rotation differently. Their workspaces are hence different.

A. Workspace with Bilateral Constraint

When the UFM is fixed in the middle, the constrained section is fixed. The free section turns to a new UFM, taking the constrained joint as the base. The end effector position and orientation can be determined as in the previous section. For the free section, the maximum joint rotation remains the same. The end effector trajectory is shown by Equation (13). In the equation, $\theta_{\min}$ and $\theta_{\max}$ are the minimum and maximum joint rotation.

$$(x-x_{N'})^2+(y-y_{N'})^2=\left(\frac{L''\cdot\sin(N''\theta''/2)}{N''\cdot\sin(\theta''/2)}\right)^2 \quad \theta_{\min}\le\theta''\le\theta_{\max} \tag{13}$$

The constraint position is controllable. As a result the UFM workspace with BC is the collection of all the possible trajectories. Figure 5 shows the workspace of a UFM with single BC. It is obvious that, compared to the workspace without constraints (dashed curve), the workspace with single BC is greatly expanded (shaded region).

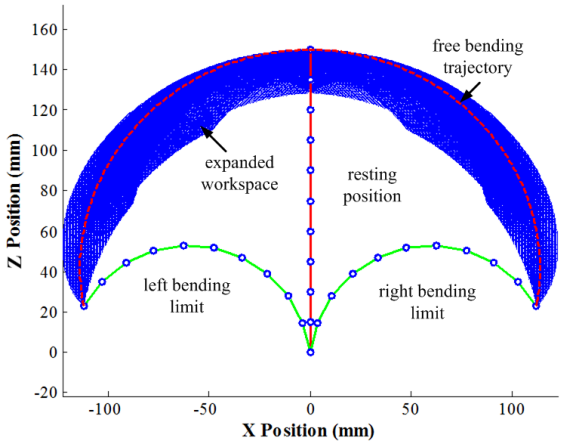

Fig. 5 Workspace with Single Bilateral Constraint

B. Workspace with Unilateral Constraint

When there is a UC, the UFM cannot cross over the constraint but can retrieve freely. The free section motion is partitioned into forward bending and backward bending. The forward bending is the same as that with BC and the backward bending is the same as that without constraint. Assume the UC locates in the right plane, i.e. $x_{N'}>0$, the end effector trajectory with a single UC is as per Equation (14).

$$\begin{cases}(x-x_{N'})^2+(y-y_{N'})^2=\left(\dfrac{L''\cdot\sin(N''\theta''/2)}{N''\cdot\sin(\theta''/2)}\right)^2 & \theta'<\theta''\le\theta_{\max}\\ (x-x_b)^2+(y-y_b)^2=\left(\dfrac{L\cdot\sin(N\theta/2)}{N\cdot\sin(\theta/2)}\right)^2 & \theta_{\min}\le\theta\le\theta'\end{cases} \tag{14}$$

When the constraint locates in the left plane, i.e. $x_{N'}<0$, the workspace has the same form with joint rotation range as: $\theta_{\min}\le\theta''<\theta'$ in the first part and $\theta'\le\theta\le\theta_{\max}$ in the second part. The workspace with UC is also the collection of all the possible trajectories.

Figure 6 shows the workspace of the UFM with a single UC. In this case the workspace is also expanded a lot. It is noted that, the workspace under UC is bounded by the free

bending trajectory. It is a subspace of the workspace with BC.

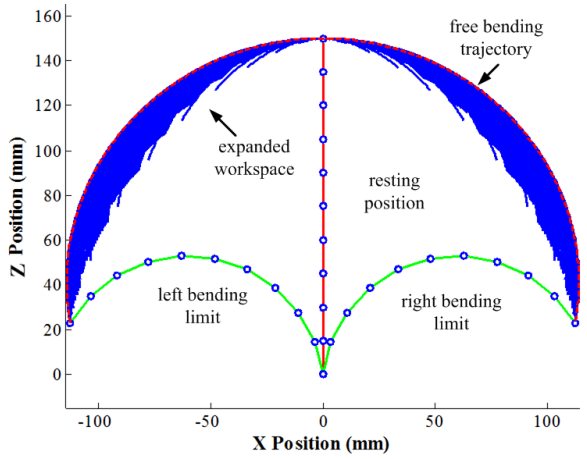

Fig. 6 Workspace with Single Unilateral Constraint

When the UFM is confined by multiple constraints or hybrid constraints the forward kinematics, inverse kinematics and workspace can be solved in a similar way.

V. Experiments and Discussions

A wire-driven underactuated serpentine manipulator is built to test the proposed idea. The prototype has 10 identical vertebras (or link). The length of each link is 15 mm, and the maximum joint rotation is 14.25º. Specifics of the UFM are shown in [9]. In the experiments, trajectory of the end effector is recorded using a grid paper as shown in Figure 7.

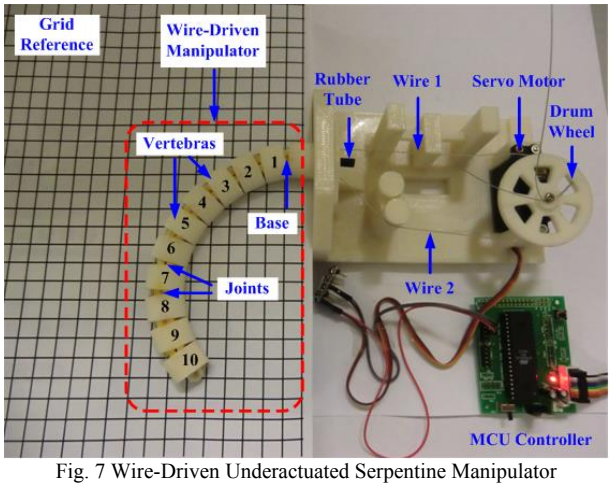

Fig. 7 Wire-Driven Underactuated Serpentine Manipulator

Two experiments are carried out. In the first experiment, the trajectory of the end effector under one BC is recorded and compared with that of model prediction. In the second experiment, the end effector trajectory under multiple UCs is compared with simulated trajectory.

A. End Effector Trajectory with Bilateral Constraint

In this experiment, the trajectory with one BC is measured and compared with model prediction. In the experiment the BC is applied by pinning a needle to the joint rotate center.

Figure 8 shows the results. In the figure, the curves are the predicted end effector trajectory; the diamonds are the recorded positions along the path; the squares are the BCs; the circles are the joints; and the polylines are the bending limits of the USM in different cases. Five cases are shown. In the first case, the USM bends freely. In case 2, the USM is pinned at the fifth joint when it is at the resting position. In case 3, the USM is pinned at the third joint when it is at the resting position. In case 4, the USM is pinned at the fifth joint when it is at the left bending limit. In case 5, the USM is pinned at the third joint when it is at the right bending limit. From the figure, the model well predicts the end effector trajectory with one BC in all the cases. When the USM is pinned at the resting position, the altered trajectory is bounded by the free bending trajectory. When the USM is pinned at the bended position, the altered trajectory crosses the free bending trajectory. Although the trajectory with single BC is shortened compared to the free bending trajectory, by actively controlling the BC position, the workspace of the USM can be expanded a lot.

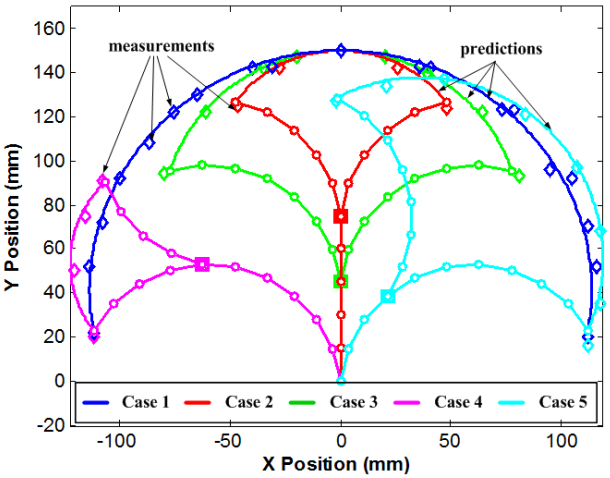

Fig. 8 End Effector Trajectory with single BC

B. End Effector Trajectory with Unilateral Constraint

In this experiment the method of predicting the end effector trajectory with multiple UCs is tested. Results are as shown in Figure 9. UCs are randomly placed on the bending plane as shown by the squares. In the beginning, the UFM is at resting position as shown by the magenta lines. By controlling the wire pair, the UFM bends to both sides. When contacting with the constraint, the joints between the constraint and the robot base stops rotating. The other joints rotate continuously until reaching the limit. As shown in the figure, in the left half plane, the first three vertebras are confined by the constraints; in the right half plane, the first five vertebras are confined by the constraints. The end effector trajectory under UCs is as shown by the red curve. The blue curve is the free bending trajectory. The diamonds are the recorded positions. Results show that the model well predicts the end effector trajectory with UCs. The altered trajectory is bounded by the free path.

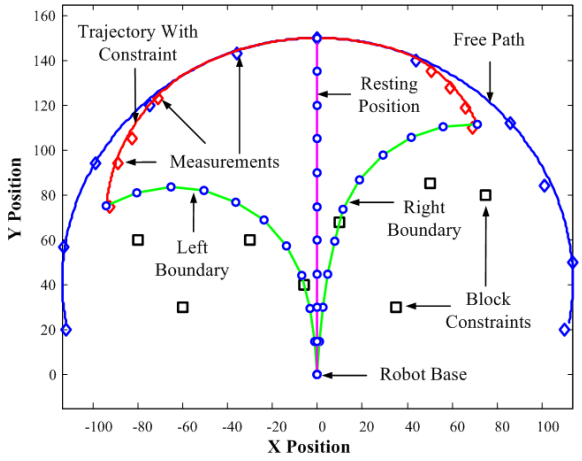

Fig. 9 End Effector Trajectory with Multiple UCs

C. Discussions

From the results, it is shown that the end effector trajectory of the USM is altered by the constraints a lot, either under single BC or multiple UCs. The changed trajectories are well predicted by the proposed method. With the aid of constraints, the end effector can reach a lot more positions.

In engineering inspection and disaster relief, it is always desirable that the end effector can reach more positions or reach a position with more orientation options. Obstacles in these applications, such as pipelines, debris, etc., are usually solid and immobile. By taking advantage of these obstacles, the manipulator workspace can be expanded a lot. Generally, these obstacles are UCs. From the analysis, the workspace expansion is smaller than that of BC. In practice, how can we make the most of constraints? If we can deploy BC actively, the UFM has the largest workspace. This can not only expand UFM workspace to the largest, but more importantly, the UFM workspace can be expanded in cases where external obstacles are soft or not allowed to touch, such as tissues.

One way is to stiffen the UFM partially. One example is the HARP robot developed in MCU [20]. It uses one inner tube to lock the posterior part of the manipulator. This is similar to deploying the BC. Another way is using smart materials, such as Magnetorheological (MR) fluid. Under magnetic field, the MR fluid becomes viscoelastic solid. The yield stress of the stiffened structure can be enhanced well above 800 kPa. By filling the tube with MR fluid and controlling the magnetic field, one can control the rigidity of the tube as well as the length of the stiffened part.

VI. Conclusion

In this paper, a novel idea of using obstacles to expand the UFM workspace is proposed. Method of deploying obstacles to reach a target position with desired orientation is also provided. The constraints are divided into two categories: UC and BC. The UFM workspace can be expanded by either constraint. The idea is validated by a wire-driven serpentine robotic arm. Simulations and experiments show that the workspace is expanded a lot. The workspace with UC is a subspace of the workspace with BC. The proposed idea is useful in applications that a large workspace is needed in confined space, such as minimally invasive surgery, disaster relief, and engineering inspection.

References

[1]R. J. Webster and B. A. Jones, "Design and Kinematic Modeling of Constant Curvature Continuum Robots: A Review," International Journal of Robotics Research, vol. 29, pp. 1661-1683, Nov 2010.
[2]J. K. Hopkins, B. W. Spranklin, and S. K. Gupta, "A survey of snake-inspired robot designs," Bioinspiration & Biomimetics, vol. 4, Jun 2009.
[3]M. Vande Weghe, D. Ferguson, and S. S. Srinivasa, "Randomized path planning for redundant manipulators without inverse kinematics," in Humanoid Robots, 2007 7th IEEE-RAS International Conference on, 2007, pp. 477-482.
[4]G. Granosik, M. G. Hansen, and J. Borenstein, "The OmniTread serpentine robot for industrial inspection and surveillance," Industrial Robot: An International Journal, vol. 32, pp. 139-148, 2005.
[5]R. H. Sturges and S. Laowattana, "A flexible, tendon-controlled device for endoscopy," The International journal of robotics research, vol. 12, pp. 121-131, 1993.
[6]P. E. Dupont, J. Lock, B. Itkowitz, and E. Butler, "Design and control of concentric-tube robots," Robotics, IEEE Transactions on, vol. 26, pp. 209-225, 2010.
[7]H. Arai and S. Tachi, "Position control system of a two degree of freedom manipulator with a passive joint," Industrial Electronics, IEEE Transactions on, vol. 38, pp. 15-20, 1991.
[8]G. Oriolo and Y. Nakamura, "Control of mechanical systems with second-order nonholonomic constraints: Underactuated manipulators," in Decision and Control, 1991., Proceedings of the 30th IEEE Conference on, 1991, pp. 2398-2403.
[9]Z. Li, R. Du, M. C. Lei, and S. M. Yuan, "Design and Analysis of a Biomimetic Wire-Driven Robot Arm," in Proceedings of the ASME 2011 International Mechanical Engineering Congress & Exposition, 2011, pp. 11-17.
[10] Y.-K. Zhu, G.-Y. Tian, R.-S. Lu, and H. Zhang, "A review of optical NDT technologies," Sensors, vol. 11, pp. 7773-7798, 2011.
[11] R. Buckingham and A. Graham, "Dexterous manipulators for nuclear inspection and maintenance—Case study," in Applied Robotics for the Power Industry (CARPI), 2010 1st International Conference on, 2010, pp. 1-6.
[12] V. Duindam, R. Alterovitz, S. Sastry, and K. Goldberg, "Screw-based motion planning for bevel-tip flexible needles in 3D environments with obstacles," in Robotics and Automation, 2008. ICRA 2008. IEEE International Conference on, 2008, pp. 2483-2488.
[13] W. McMahan, B. A. Jones, and I. D. Walker, "Design and implementation of a multi-section continuum robot: Air-Octor," in Intelligent Robots and Systems, 2005.(IROS 2005). 2005 IEEE/RSJ International Conference on, 2005, pp. 2578-2585.
[14] V. D. Sars, S. Haliyo, and J. Szewczyk, "A practical approach to the design and control of active endoscopes," Mechatronics, vol. 20, pp. 251-264, 2010.
[15] C. Laschi, B. Mazzolai, V. Mattoli, M. Cianchetti, and P. Dario, "Design of a biomimetic robotic octopus arm," Bioinspiration & Biomimetics, vol. 4, p. 015006, 2009.
[16] Z. Li and R. Du, "Design and Analysis of a Bio-Inspired Wire-Driven Multi-Section Flexible Robot," Int J Adv Robotic Sy, vol. 10, 2013.
[17] J. M. Croom, D. C. Rucker, J. Romano, and R. Webster, "Visual sensing of continuum robot shape using self-organizing maps," in Robotics and Automation (ICRA), 2010 IEEE International Conference on, 2010, pp. 4591-4596.
[18] A. Bajo, R. E. Goldman, and N. Simaan, "Configuration and joint feedback for enhanced performance of multi-segment continuum robots," in Robotics and Automation (ICRA), 2011 IEEE International Conference on, 2011, pp. 2905-2912.
[19] A. Bajo and N. Simaan, "Kinematics-Based Detection and Localization of Contacts Along Multisegment Continuum Robots," Ieee Transactions on Robotics, vol. 28, pp. 291-302, Apr 2012.
[20] A. Degani, H. Choset, A. Wolf, T. Ota, and M. A. Zenati, "Percutaneous intrapericardial interventions using a highly articulated robotic probe," 2006, pp. 7-12